Pressure effect on magnetic and magnetotransport properties of intermetallic and colossal magnetoresistance oxide compounds

2005 J. Phys.: Condens. Matter 17 S3035

(http://iopscience.iop.org/0953-8984/17/40/007)

INSTITUTE OF PHYSICS PUBLISHING JOURNAL OF PHYSICS: CONDENSED MATTER

J. Phys.: Condens. Matter **17** (2005) S3035–S3055 doi:10.1088/0953-8984/17/40/007

Pressure effect on magnetic and magnetotransport properties of intermetallic and colossal magnetoresistance oxide compounds

Z Arnold[1,4], M R Ibarra[2], P A Algarabel[2], C Marquina[2], Jose María De Teresa[2], L Morellon[2], J Blasco[2], C Magen[2], O Prokhnenko[1], J Kamarád[1] and C Ritter[3]

[1] Institute of Physics AS CR, Na Slovance 2, 182 21 Prague 8, Czech Republic
[2] Departamento de Física de la Materia Condensada and Instituto de Ciencia de Materiales de Aragón, Universidad de Zaragoza and Consejo Superior de Investigaciones Científicas, 50009 Zaragoza, Spain
[3] Institut Laue-Langevin, Boîte Postale 156, 38042 Grenoble Cédex 9, France

E-mail: arnold@fzu.cz

Received 8 July 2005
Published 23 September 2005
Online at stacks.iop.org/JPhysCM/17/S3035

Abstract

The joint power of neutron diffraction and pressure techniques allows us to characterize under unique conditions the nature and different role of basic interactions in solids. We have covered a broad phenomenology in archetypical compounds: intermetallics and magnetic oxides. We have selected compounds in which the effect of moderate pressure is able to modify the electronic structure and bond angles that in turn are in the bases of magnetic and structural transitions. Complex magnetic and structural phase diagrams are reported for compounds with magnetic ($Tb_{1-X}Y_XMn_2$) and structural ($RE_5Si_{4-X}Ge_X$) instabilities. Pressure-induced change of the magnetic structure in (R_2Fe_{17}) intermetallics and the effect on the colossal magnetoresistance manganites are described.

1. Introduction

A systematic study of the basic magnetic properties' dependence (magnetic moments, magnetic structures, temperatures of magnetic ordering, magnetotransport) on interatomic distances in magnetic rare earths and transition metal alloys and oxide compounds is very helpful in order to understand a large variety of phenomena such as Invar behaviour, magnetic instabilities, and magnetostructural and metal–insulator transitions. Many f and d electron systems exhibit large magnetovolume and magnetoelastic effects under multiextreme conditions: under high pressures, low temperatures and high magnetic fields [1]. The decrease of the magnetic

[4] Address for correspondence: Department of Magnetics and Superconductors, Institute of Physics AS CR, Cukrovarnicka 10, 162 53 Praha 6, Czech Republic. http://www.fzu.cz/~arnold/.

moments under high pressure is a general trend in the magnetic behaviour of solids with only a few exceptions. This trend is especially relevant in the 3d metallic magnets. Theoretical calculations showed that, in general, the pressure effects could be attributed to increasing hybridization of the electrons and to the broadening of the energy bands. The splitting of the d-band depends on both the increasing interaction energy and the decreasing density of states. Among the members of the 3d-series, the rate of the band broadening normally predominates over the increase in the interaction between the itinerant electrons and the band magnetism is destroyed under high enough pressures [2]. Moreover, the members of the 4f-series, lanthanides, are the most successful in retaining their atomic magnetism. The 4f shell is relatively closely bound to the nucleus of the atom, and so the electrons are shielded by the outer $5s^2$–$5p^6$ electrons and, to some extent, by the three 5d–6s valence electrons. This leads to the negligible orbital overlap and the well-localized and stable nature of the magnetic state. Magnetic oxides present an ionic core magnetic moment, which interacts by indirect mechanisms such as superexchange and double exchange. The colossal magnetoresistance (CMR) mixed valent manganites are characterized by the existence of Mn in two ionic states: Mn^{4+} (t_{2g}^3) and Mn^{3+} ($t_{2g}^3 e_g^1$). The high spin configuration (which is the ground state) provides t_{2g} core magnetic moments ($\mu = 3\ \mu_B$) which ferromagnetically interact through the itinerant e_g electron, i.e. the double exchange interaction. The intensity of this interaction is mediated by the relative orientation of the core magnetic moments: for the parallel orientation, i.e. ferromagnetic alignment of the e_g, the electron transfer is maximum and the system is metallic; however, in the case of either magnetic disorder or antiferromagnetic alignment the electron itinerancy is suppressed, and an insulator state results [3].

Neutron diffraction experiments under high pressures are relevant for obtaining information about the nature of the relations between the changes of volume and magnetic structures. We present in this short review several examples of compounds with localized magnetic moments, namely the $(La_{1-x}Nd_x)_{2/3}Ca_{1/3}MnO_3$ manganites and $Tb_5Si_2Ge_2$ magnetocaloric compounds and Y_2Fe_{17} and $Tb_{1-X}Y_XMn_2$ compounds that represent compounds with itinerant magnetism.

Pioneer works [4, 5] on the pressure effect on CMR mixed valent manganites revealed an increase of the Curie temperature (T_C) with pressure. This was related to the corresponding increase of the Mn–O–Mn bond angle [6] that in turn enhances the ferromagnetic double exchange interaction. The combined effect of pressure and oxygen isotopic mass exchange are reported in $(La_{1-x}Nd_x)_{2/3}Ca_{1/3}MnO_3$ in which a delicate balance among interactions—ferro (double exchange) antiferro (superexchange) and charge ordering—controls the existence of a ground state based in the existence of a phase segregation of metallic (ferro) and insulator regions (antiferro). In the RMn_2 intermetallics the existence of local moment on the Mn ions critically depends on the interatomic distances [7]. Neutron diffraction experiments under pressure performed in $Tb_{1-X}Y_XMn_2$ were relevant in order to understand the mechanism for the appearance of magnetic instabilities on the 3d magnetism. We also report the relevant role of the lattice effect which drives the giant magnetocaloric effect found in $Tb_5Si_2Ge_2$ [8]. A large variety of magnetic and structural phases was found for different Si and Ge concentration that could be modulated by applied pressure. Finally, we describe an archetypical example of the lattice effect on the 3d magnetism, which is the case of R_2Fe_{17} [9] in which pressure can suppress a ferromagnetic ground state and induce a non-collinear magnetic structure.

2. Experimental details

To determine the relation between the pressure and volume at different temperatures, measurements of compressibility and linear thermal expansion (LTE) were performed within

the temperature range 10–300 K. The measurements were carried out by a strain gauge [10] method. These experiments were performed in piston cylinder CuBe pressure cells together with a closed cycle refrigerator under hydrostatic pressure up to 10 kbar [11]. The results on selected samples were complemented by the direct measurements of thermal dependence of lattice parameters using the results of temperature dependence of neutron diffraction under pressure.

The measurements of the magnetic properties (magnetization, magnetocrystalline anisotropy, and ordering temperatures) under pressure were performed in a SQUID magnetometer (up to 5 T) in a temperature range 4–300 K using a miniature CuBe pressure cell up to 12 kbar [11].

The neutron diffraction experiments under pressure were carried out at the Institute Laue Langevin (Grenoble). The double-axis multicounter diffractometer D1B using 2.52 Å wavelength supplemented either with standard continuously loaded He gas high-pressure cell up to 5 kbar or with clamp pressure cells was used for the measurements. The use of a continuously loaded pressure cell allowed us to keep the pressure constant during temperature changes and to perform pressure scans at constant temperature. The high-intensity D20 diffractometer was used for the pressure studies of the $Tb_5Si_2Ge_2$ sample. High-resolution diffractometers D1A and D2B were used to characterize the ground states of the studied materials. Recent pressure studies on single-crystalline samples were performed at the HMI Berlin on E4 diffractometer, where a clamp pressure cell with a mixture of mineral oils as the pressure transmitting medium was used. The data analysis was done using the FULLPROF refinement package [12].

3. Results and discussion

3.1. Pressure and isotope effects in $La_{2/3}Ca_{1/3}MnO_3$ and $La_{1/35}Nd_{1/3}Ca_{1/3}MnO_3$ manganites

The physics in manganites has primarily been described by the double-exchange (DE) model [13, 14]. There are indications that double exchange alone cannot fully explain the data of $La_{2/3}Ca_{1/3}MnO_3$ (and related compounds) and that lattice-polaronic effects due to strong electron–phonon coupling (arising from a strong Jahn–Teller effect) should be involved [15]. It is widely accepted that the ferromagnetic transition in $La_{2/3}Ca_{1/3}MnO_3$ (and related compounds) is simultaneous with an insulator–metal transition [16, 17]. The strong coupling between the electronic and lattice subsystems have been demonstrated by the observation of a giant oxygen-isotope shift of the ferromagnetic transition temperature T_C in $La_{1-X}Ca_XMnO_3$ [18]. The scenario is also supported by thermal-expansion [19, 20] and small-angle neutron scattering experiments [21]. It was also suggested in [22] that magnetic polarons (consisting of an electron that polarizes the magnetic moment around it) should be involved in order to explain their results of the resistivity and neutron-scattering experiments.

The intensity of the ferromagnetic interaction is closely correlated with the structural parameters as well as with the lattice dynamics through the electron–phonon (e–ph) interaction. The bare electronic e_g bandwidth is determined by the Mn–O–Mn bond angle, being maximum for Mn–O–Mn $= 180°$. Consequently, the Zener interaction is reduced as the structure becomes more distorted. Hwang *et al* [16] and De Teresa *et al* [23] found a phase diagram in which, for the highly distorted structures, the long-range ferromagnetic ordering is suppressed and a spin-glass (or cluster-glass) state can appear at low temperatures due to the competition between the ferromagnetic (F) and antiferromagnetic (AF) interactions. An increase in the e–ph interaction has been found to weaken the F interaction [24]. In addition, the long-range Coulomb interaction between electrons gives rise to Mn^{4+}/Mn^{3+} charge ordering (CO) in some

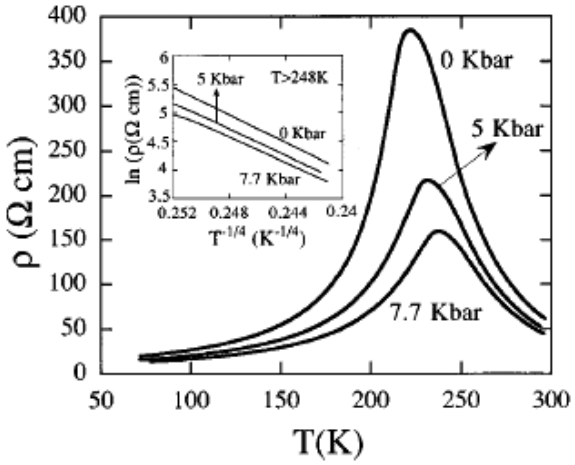

Figure 1. Resistivity (ρ) as a function of temperature under pressure values of 0, 5, and 7.7 kbar in $La_{2/3}Ca_{1/3}MnO_3$. The inset shows ln ρ versus $T^{-1/4}$ at temperatures above T_c [21].

mixed-valence manganites [25]. The ground state of a manganite is a subtle balance of the F, AF, CO, and e–ph interactions, which can be easily modified by chemical substitution, isotopic exchange, external pressure and magnetic field.

The effect of pressure on the properties of $La_{2/3}Ca_{1/3}MnO_3$ is not obvious to predict [15, 26]. In figure 1 we present the resistivity results under pressures of 0, 5, and 7 kbar. The resistivity decreases with pressure across the whole range of temperatures. In the inset of figure 1, we have plotted ln ρ versus $T^{-1/4}$ to check if conduction by magnetic polarons takes place under such pressures. The curves are linear, which suggests that up to 7.7 kbar the conduction is via magnetic polarons above T_C. The increase of the T_C by applying pressure is a consequence of the enhancement of the DE interaction, responsible for the ferromagnetism in this compound. The strength of the DE interaction is measured through the transfer integral between neighbouring Mn sites, $t_{\mathrm{eff}} = t_0 \cos(\Theta/2)$. As t_0 depends on the length and angle of the Mn–O bond, it is expected to be strongly pressure dependent.

In figure 2, we present the AC susceptibility and the volume thermal expansion under pressure. From the AC susceptibility we obtain the slope of the insulator–metal transition temperature (which coincides with T_C) dependence with pressure: $\mathrm{d}T_C/\mathrm{d}P = 2.2$ K kbar^{-1}. The values of T_C obtained from the AC susceptibility measurements for all the pressures coincide with the maxima of the resistivity curves. The volume anomaly bound to the insulator–metal transition is shifted by pressure in the same way as the electrical and the magnetic anomaly. Moreover, the volume change at T_C is reduced with increasing pressure. This is a consequence of the incomplete charge localization above T_C when pressure is applied. Then there is less charge to be delocalized at T_C and the drop diminishes.

The series $(La_{1-x}Nd_x)_{2/3}Ca_{1/3}MnO_3$ is an example of the subtle balance of the F, AF, CO, and e–ph interactions. For $x < 0.5$ there are para–ferromagnetic and Metallic (Mt)–Insulating (In) transitions [27], whereas for $x > 0.5$ there is no Mt–In transition and the compound with $x = 1$ has been characterized as CO [28]. The $x = 0.5$ compound is just on the border, and macroscopic measurements seem to indicate that its ground state at low temperature is 'anomalous' [21]. That is the reason why we have chosen such a composition to study the isotopic exchange.

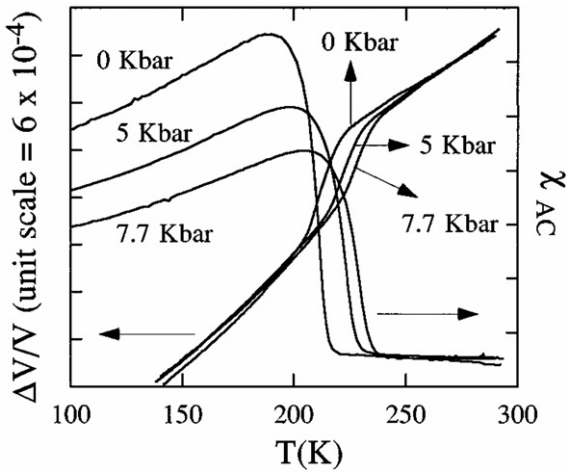

Figure 2. The AC susceptibility (χ_{ac}) and volume thermal expansion ($\Delta V/V$) as a function of temperature at pressure values of 0, 5, and 7.7 kbar in $La_{2/3}Ca_{1/3}MnO_3$ [21].

Zhao *et al* [29] have shown a strong effect of the oxygen mass on the magnetic and transport properties in the compound $(La_{0.5}Nd_{0.5})_{2/3}Ca_{1/3}MnO_3$. The compound with the ^{18}O isotope is an insulator over the whole temperature range, whereas the ^{16}O sample exhibits an Mt–In transition at ≈150 K. In order to gain more insight into the role of the e–ph interaction to determine the ground state in the mixed valence manganites and how it changes with various internal and external parameters, we have performed resistivity, thermal-expansion, magnetostriction, and neutron-diffraction measurements on the oxygen-isotope exchanged samples of $(La_{0.5}Nd_{0.5})_{2/3}Ca_{1/3}MnO_3$ under high magnetic fields and hydrostatic pressures.

The volume thermal expansion for the ^{16}O and ^{18}O samples of $(La_{0.5}Nd_{0.5})_{2/3}Ca_{1/3}MnO_3$ (denoted as ^{16}O and ^{18}O) is shown in figure 3. For comparison, we also include the results for the ^{16}O samples of $La_{2/3}Ca_{1/3}MnO_3$ and $Pr_{2/3}Ca_{1/3}MnO_3$. The solid line represents the phonon contribution calculated from the Grüneisen law using a Debye temperature (Θ_D) of 500 K. The extra anharmonic contribution with respect to the phonon contribution has been associated with the carrier localization due to polaronic effects [30]. We have chosen the volume thermal expansion curve of the compound $Pr_{2/3}Ca_{1/3}MnO_3$ [31] as a prototype for the insulating state, whereas the result of $La_{2/3}Ca_{1/3}MnO_3$ at low temperatures is representative of the metallic state [21].

At $T \approx 200$ K, anomalies in the linear thermal-expansion coefficient of both ^{16}O and ^{18}O samples, which are characteristic of CO [31], are present (see the inset of figure 3). The CO temperature seems to be independent of the isotopic mass. The thermal expansion for the ^{18}O sample follows the insulating behaviour over the whole temperature range, which indicates that the insulating CO state is stable down to the lowest temperature. There is no Mt–In transition, in good agreement with previous electrical resistivity measurements [29]. In contrast, the ^{16}O sample shows a different behaviour. Above 150 K, the thermal expansion curve corresponds to the insulating behaviour, and below this temperature, the curve falls in between those for the insulating and metallic states. This result suggests that at low temperature insulating CO and metallic F regions coexist in the ^{16}O sample of $(La_{0.5}Nd_{0.5})_{2/3}Ca_{1/3}MnO_3$, whereas the ^{18}O sample has a homogeneous CO state.

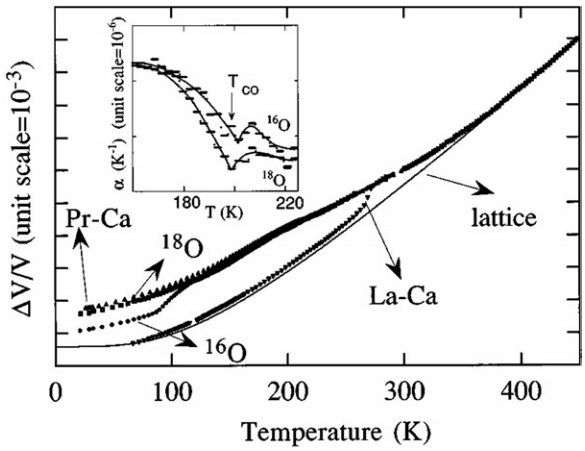

Figure 3. Comparison of the ^{16}O (dots) and ^{18}O (squares) volume thermal expansion with prototype insulating ($Pr_{2/3}Ca_{1/3}MnO_3$) (triangles) and metallic (low-temperature $La_{2/3}Ca_{1/3}MnO_3$) (inverted triangles) compounds. 'Lattice' stands for the calculated phonon contribution using the Grüneisen law (line). The inset shows the linear thermal expansion coefficient for the ^{16}O and ^{18}O samples in the vicinity of T_{CO} [32].

The results of the volume magnetostriction at selected temperatures that clearly indicate remarkable different values below ≈100 K for the both samples can be interpreted [32] in such a way that in the absence of applied field the CO phase extends over a large volume fraction of the ^{18}O sample in comparison with the ^{16}O sample. At 50 K and at fields higher than 5 T, the magnetostriction in the ^{18}O sample is twice the value found under the same conditions in the ^{16}O sample. This gives rise to a huge isotopic effect on the volume magnetostriction. These results indicate a higher stability of the CO state in the ^{18}O sample than in the ^{16}O sample.

The pressure effect on the electrical resistivity is shown in figure 4 for the two isotopic samples. For the ^{18}O sample, there is no significant effect under pressures up to 9 kbar. There is a weak anomaly at T_{CO} and an insulating behaviour over the whole temperature range. The absolute value of the resistivity depends weakly on the pressure. However, the sample ^{16}O displays an Mt–In insulator transition, as seen from the peak-like anomaly, and the pressure effect is very large. These results in the ^{16}O sample are in good agreement with those reported by Zhou *et al* [28]. The different behaviour of the low-temperature resistivity under pressure in both isotope exchanged samples can be explained by the important role of the phase segregation in the ^{16}O sample.

In order to confirm the possible existence of AF order in the CO region, we performed neutron diffraction experiments in both isotopic samples. Neutron-diffraction spectra taken at different temperatures showed several relevant features. A small superstructure peak appears at $T_{CO} \approx 210$ K (hereafter called the CO peak), which coincides with the temperature at which the anomaly in thermal expansion and resistivity is found. An extra contribution over the Bragg nuclear peaks is observed, which reveals the presence of an F phase below $T_C \approx 200$ K. The existence of an extra peak of magnetic origin indicates the existence of an AF phase below $T_{AF} \approx 170$ K. We consider that the long-range AF order occurs within the CO region.

In figure 5 we show the thermal dependence of the integrated intensity of selected CO, F, and AF peaks. The appearance of the CO peak indicates the transition from paramagnetism to CO in the ^{18}O sample. In the case of ^{16}O this transition takes place only in a small part of the sample, the CO peak being too small to be refined. The AF phase sets in at T_N. The intensity

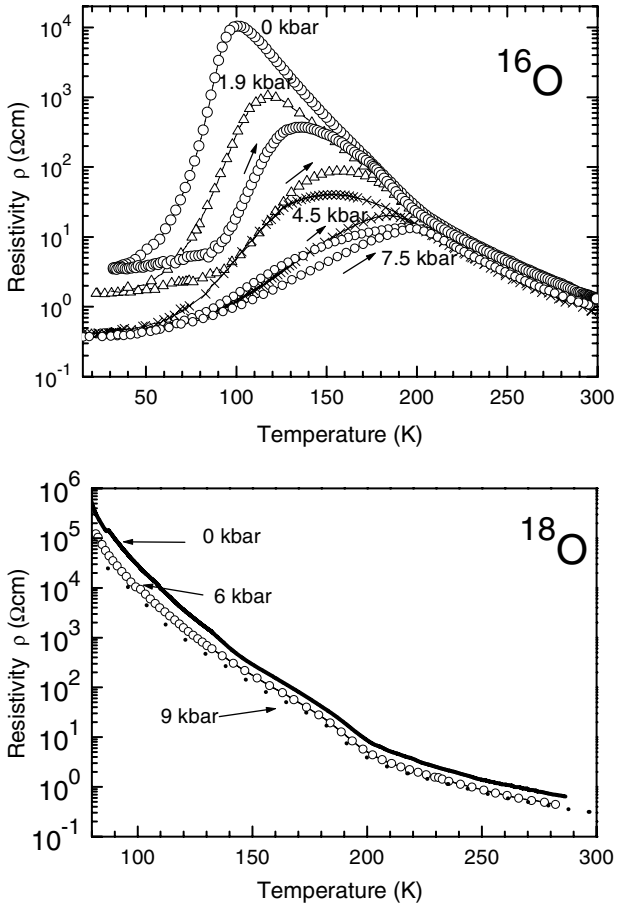

Figure 4. Thermal dependence of the electrical resistivity at several selected pressures in ^{16}O and in ^{18}O [32].

of the AF peak in the ^{18}O sample, where CO is the majority phase, is very large in comparison with the ^{16}O sample. This is consistent with the existence of a para–AF transition within the CO region. The results for the F peak, shown in the inset of figure 3, are an indication of the presence of a majority F phase in the ^{16}O sample, which is almost imperceptible in the ^{18}O sample. The small F contribution found in this sample can be associated with the ^{16}O-rich region in which the isotopic exchange was not achieved.

In summary, we have found a very large isotopic effect on the magnetic, magnetotransport, and magnetoelastic properties of the mixed-valence manganite $(La_{0.5}Nd_{0.5})_{2/3}Ca_{1/3}MnO_3$, where a subtle energy balance makes this compound phase segregated. We have found that the CO temperature does not change. Therefore, we propose that the long-range Coulomb interaction, responsible for the CO, is not affected by the change in the oxygen isotopic mass. Considering the large effect of the isotopic change on the phase segregation, we conclude that the weakening of the Zener interaction due to a strong electron phonon interaction existing in these compounds is responsible for the observed effects. The pressure experiments can be explained in a similar way. It is well established that pressure enhances the Zener interaction. Therefore, the effect on the phase segregation is opposite to the effect by isotopic exchange.

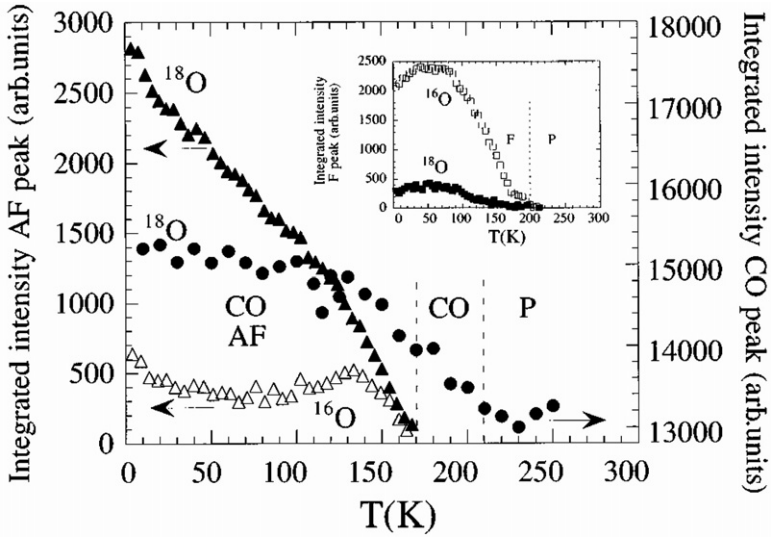

Figure 5. Thermal dependence of the integrated intensity of the superstructure peak (CO) (dots) and (1/2, 0, 0) and (0, 1/2, 0) antiferromagnetic (AF) peak (triangles), characteristic of the insulating CO region. Inset: thermal dependence of the ferromagnetic (F) contribution to the (0, 0, 1) and (1, 1, 0) Bragg peak, which characterizes the metallic F region (squares). P means paramagnetic. Open symbols stand for the ^{16}O sample and closed symbols for the ^{18}O sample [32].

Under pressure, the ferromagnetic phase is favoured with respect to the CO, resulting in a decrease of the resistivity under pressure. However, the effect is not large enough in the ^{18}O sample to produce an In–Mt transition.

3.2. Magnetic phase diagram of $Tb_{1-X}Y_XMn_2$ compounds

There are many magnetic systems that show volume changes associated with a first-order magnetic phase transition in which the magnitude of the magnetic moment changes. This behaviour appears in very different systems such as FeRh [33] (where the antiferromagnetic–ferromagnetic transition is accompanied by stabilization of the Rh magnetic moment), $CeNi_{1-x}Co_xSn$ [34] (with a first-order Ce valence change). One interesting family of compounds is the RMn_2, in which a stabilization of magnetic moment at the Mn sites takes place at low temperatures [35]. In all these systems, there exists a strong link between magnetism and lattice that brings about large instabilities induced by external parameters such as the magnetic field or pressure [33–36].

YMn_2 shows strong spin fluctuations; at T_N (≈70–100 K) there is a first-order transition, with a volume change associated with the appearance of a local moment at the Mn sites. Mn magnetic moments (2.8 μ_B) order in an antiferromagnetic helix [37, 38] (this structure will be called AF1 hereafter). $TbMn_2$ also shows a first-order volume change when the Mn acquires a local moment at $T_N \approx 45$ K. The Tb and Mn magnetic moments are arranged in an antiferromagnetic structure [39, 40] (called AF2 hereafter). Consequently, new magnetic states can also be expected across the $Tb_xY_{1-x}Mn_2$ series.

Due to the strong magnetic instabilities in the $Tb_{1-X}Y_XMn_2$ compounds, the effect of applying magnetic field or pressure is expected to be large. An applied pressure of 3 kbar avoids the appearance of magnetic moment at the Mn sites in YMn_2 and $TbMn_2$ [37]. At

lower pressures, there is a coexistence of two phases: a transformed phase with local magnetic moment at the Mn sites and a non-transformed phase with itinerant Mn moments. The transformed phase is unstable under an external magnetic field in $TbMn_2$ while it is stable in YMn_2 [35].

Based on the results of macroscopic measurements (linear thermal expansion, AC susceptibility under pressure up to 7 kbar and magnetostriction up to 14 T) preliminary magnetic phase diagrams for the transformed and non-transformed phases of the $Tb_xY_{1-x}Mn_2$ compounds were proposed [38]. The linear thermal expansion measurements showed that at ambient pressure all the $Tb_xY_{1-x}Mn_2$ compounds undergo a first-order volume contraction (at ≈40 K for $x \geqslant 0.2$) ranging from ≈1:5% for $x = 1$ to ≈5% for $x = 0$, which is a hallmark of the existence of the transformed phase. Measurements of AC susceptibility under pressure confirmed that the transformed phase is unstable under pressure for all the compounds. The peaks in the AC susceptibility, which appear in the Tb-rich compounds ($x \geqslant 0.6$) under pressure were associated with para–ferrimagnetic transitions within the non-transformed phase. Magnetostriction measurements allowed us to establish that for the Tb-rich compounds ($x \geqslant 0.6$) the magnetic structure is unstable under applied magnetic field, which suggested the AF2-like structure. For the Y-rich compounds ($x \leqslant 0.2$) the magnetic structure is stable under applied magnetic field, which suggested the AF1-like structure.

It was impossible to determine with our macroscopic measurements the existence of magnetic order in the compounds around the concentration $x = 0.4$. Nevertheless, neutron diffraction experiments under pressure (up to 5 kbar) provide an excellent and indispensable tool to identify the magnetic structures of both phases as well as the relative percentage of the transformed phase and non-transformed phases across the whole $Tb_xY_{1-x}Mn_2$ series at each pressure and to determine how the non-transformed phase becomes stabilized under pressure. These experiments confirmed the existence of two magnetic states very close in energy in $Tb_xY_{1-x}Mn_2$ at low temperatures. They have very different unit cell volume and magnetic structures (both associated with the transformed and non-transformed phases). We found coexistence of these two different phases under certain conditions. At ambient pressure, all compounds undergo a first-order magnetic transition, as the Mn magnetic moment becomes local, giving rise to a transformed phase. This phase with higher volume is the phase of minimum energy. Part of the sample can remain non-transformed and the two phases coexist below the transition temperature. As pressure is applied the relative volume percentages of the transformed phase and non-transformed phases change as the transformed phase becomes unstable under pressure. At intermediate pressures, the general situation is the coexistence of both phases. At higher pressures, the non-transformed phase, with itinerant Mn moments and low volume, is the phase of minimum energy, and at high enough pressures, only the non-transformed phase is present. This development of phases is illustrated in figure 6, where the neutron diffraction thermogram of $Tb_{0.8}Y_{0.2}Mn_2$ at 1 bar is visualized, and in figure 7, where the neutron diffraction thermograms of $Tb_{0.8}Y_{0.2}Mn_2$ at 1.4 kbar (a) and 2.2 kbar (b) are presented. Within the non-transformed phase, for $x > 0.2$ there is a transition to a magnetic structure that is reminiscent of the $DyMn_2$-like structure (F phase). In the transformed phase, the $TbMn_2$-like magnetic structure develops at high Tb concentrations while at low Tb concentrations two different antiferromagnetic structures are visible, a YMn_2-like structure and a new antiferromagnetic structure unknown up to now. Across the intermediate concentration range, a magnetic ground state with short-range correlations is present.

In figure 8(a) we show the magnetic phase diagram of the transformed phase according to the neutron diffraction measurements [41]. At ambient pressure for all the compounds there is a first-order phase transition when the Mn magnetic moment becomes local. The transition temperature depends on the Y content, being around 50 K for $x \geqslant 0.2$ and 90 K for $x = 0$. In

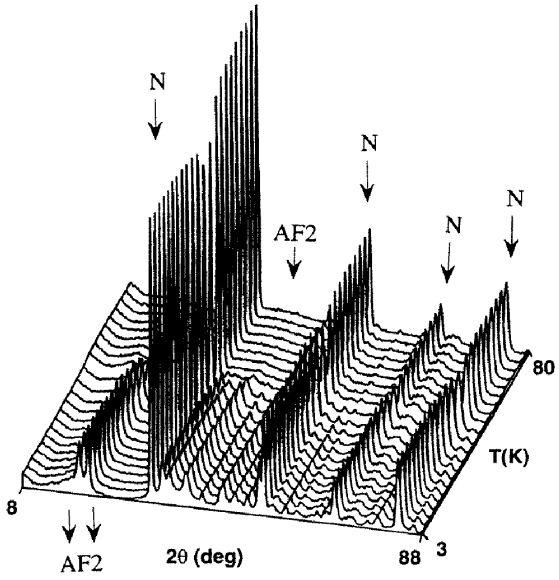

Figure 6. The neutron diffraction thermogram of $Tb_{0.8}Y_{0.2}Mn_2$ at 1 bar. The arrows indicate the origins of the peaks (N, nuclear; AF2, see the text).

the compounds with high Y content, the Mn magnetic moments order antiferromagnetically with the AF1 (YMn_2-like) structure or the unknown AF structure. For $x = 0.4$ the absence of magnetic peaks and the presence of magnetic correlations point to short-range magnetic ordering. Such correlations appear at the positions where the magnetic peaks of the AF2 ($TbMn_2$-like) structure appear. In the high-Tb-content region, the Mn magnetic moments order with the AF2 structure. When pressure is applied the transformed phase appears at lower temperatures (see in figure 8(a) that at 3 kbar the transformed phase has completely disappeared for $x \leqslant 0.2$), keeping however the same magnetic structure. In figure 8(b), we show the magnetic phase diagram of the non-transformed phase. The values of T_C have been obtained from the AC susceptibility measurements [40] as this information was less accurate when obtained with our neutron results. Two facts are relevant. First, only two magnetic states are possible at low temperatures. For high Tb content, the F ($DyMn_2$-like) structure occurs, and for high Y content, the sample remains paramagnetic. Second, as the pressure increases T_C increases. This fact is due to the reinforcement of the Tb–Tb exchange interaction with pressure. In our previous paper [38] we suggested the possibility of the loss of the long-range magnetic order in the non-transformed phase for the compounds with high enough Y concentration. The neutron results indicate that the magnetic peak width does not change with the Y content, which would be a hallmark of short-range or spin-glass magnetic behaviour. The situation can be close to a crossover from long-range to short-range order but this is not still manifested as a broadening of the neutron diffraction magnetic peaks.

We can conclude that all the experimental results in the series of intermetallic compounds $Tb_xY_{1-x}Mn_2$ under pressure can only be explained considering the existence of two phases. At ambient pressure and low temperatures, the Mn magnetic moment becomes local, giving rise to a transformed phase with a strong lattice expansion. The magnetic structure in this transformed phase is YMn_2-like for the high-Y-content region, $TbMn_2$-like for the high-Tb-content region, and short-range magnetic order of the $TbMn_2$-like structure for compounds

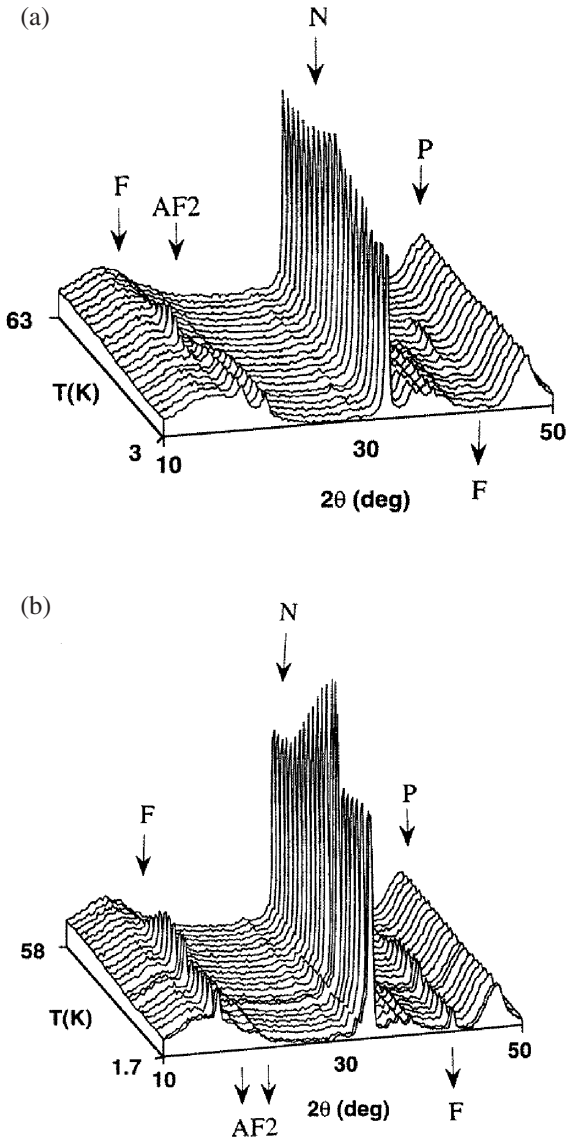

Figure 7. The neutron diffraction thermograms of $Tb_{0.8}Y_{0.2}Mn_2$ at (a) 1.4 kbar and (b) 2.2 kbar. The arrows indicate the origin of the peaks (N, nuclear; P, pressure cell, AF2 and F, see the text).

around $x = 0.4$. When pressure is applied, there is coexistence of the transformed phase and a non-transformed phase. At high pressure, only the non-transformed phase exists. The non-transformed phase orders with the $DyMn_2$-like structure for high Tb content and remains paramagnetic for low Y content.

3.3. Magnetic and structural transitions in $Tb_5Si_2Ge_2$

$R_5(Si_xGe_{1-x})_4$ (R = rare earth element) is a unique family of giant magnetocaloric effect (MCE) materials [42] where a remarkable physics has been found [43] including strong

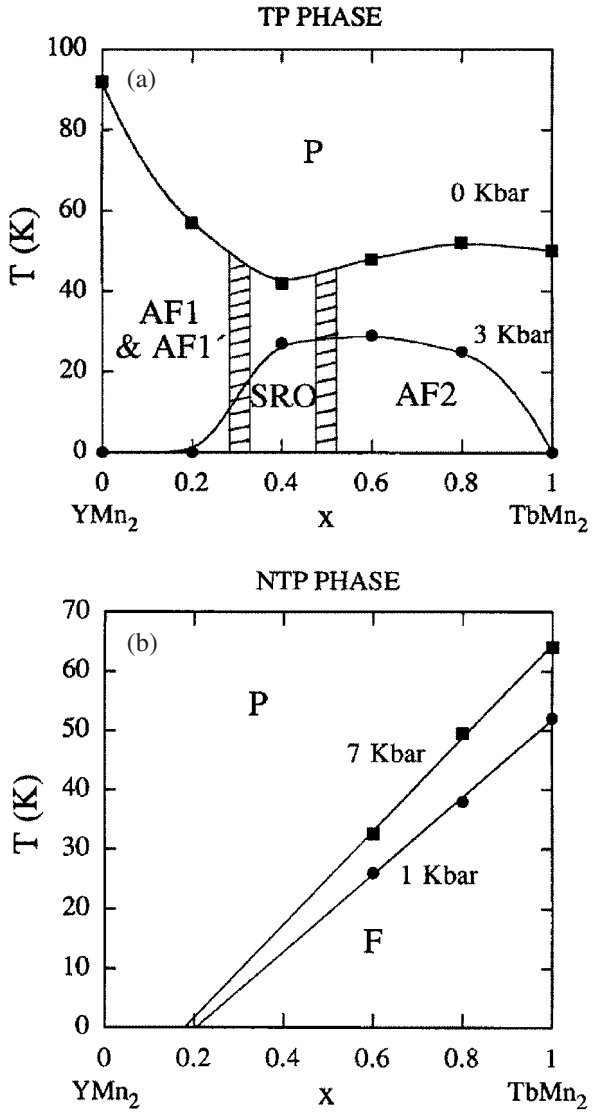

Figure 8. Magnetic phase diagrams of $Tb_xY_{1-x}Mn_2$: (a) transformed phase (TP) at 1 bar and 3 kbar according to the neutron diffraction results; (b) non-transformed phase (NTP) at 1 and 7 kbar according to the AC susceptibility results. the lines are visual guides.

magnetoelastic effects [44], and giant magnetoresistance [45]. The observed phenomenology has been associated with an intrinsically layered crystallographic structure built by stacking two-dimensional sub-nanometric-thick layers (slabs) interconnected via partially covalent interslab (Si, Ge)–(Si, Ge) bonds [46]. The formation or cleavage of these bonds by changing external parameters such as temperature, magnetic field, or hydrostatic pressure [47, 48] results in dramatic crystallographic, electronic, and magnetic changes, thus explaining the powerful magnetoresponsive properties of these materials.

The $Tb_5(Si_xGe_{1-x})_4$ series is the second best studied [49–51], in which a comprehensive neutron diffraction characterization has been possible [50, 51] due to the absence of Gd,

an element with an enormous neutron absorption cross section. The $Tb_5(Si_xGe_{1-x})_4$ alloys with intermediate compositions $0.4 \leqslant x \leqslant 0.6$ present at room temperature a paramagnetic (PM) monoclinic (M, $P112_1/a$) structure where one every other interslab covalent-like bonds are broken. The low-temperature ground state is ferromagnetic (FM) with an orthorhombic structure (O(I), $Pnma$) where all bonds are formed. Nevertheless, unlike the $Gd_5(Si_xGe_{1-x})_4$ alloys where a fully coupled first-order M(PM) $\rightarrow$ O(I)(FM) transition takes place on cooling, we reported that in $Tb_5Si_2Ge_2$ long-range ferromagnetism sets in within the monoclinic phase (M(FM)) (T_C) before the M $\rightarrow$ O(I) structural transformation (T_t) [51]. Therefore, we demonstrated that the structural and magnetic transitions are not fully coupled in this system, on cooling, the following sequence taking place: M(PM) $\rightarrow$ M(FM) $\rightarrow$ O(I)(FM).

It was observed in the compounds of the R = Gd series [47, 48], that the pressure-induced increase of the transition temperature at the second-order boundaries is rather moderate (+0.3–0.7 K kbar^{-1}), whereas this effect is significantly stronger (+3 K kbar^{-1}) at the first-order magnetostructural line. The positive values of the pressure slopes of the magnetic ordering temperatures are in agreement with a localized character of the RE magnetic moments. The effect of pressure is, therefore, that of enhancing the interlayer interactions, favouring the ferromagnetic O(I) state. Within this approach, the application of hydrostatic pressure in $Tb_5Si_2Ge_2$ should lead to a moderate increase in the second-order Curie temperature T_C, a stronger effect being expected at the first-order structural transformation T_t.

To confirm this expected behaviour we performed a comprehensive study of the temperature–pressure (T–P) phase diagram of $Tb_5Si_2Ge_2$ by means of linear thermal expansion (LTE), magnetization, and neutron powder diffraction experiments under hydrostatic pressure [52]. The use of neutron diffraction experiments under pressure was indispensable to fully characterize the different crystallographic and magnetic phases as a function of temperature.

To determine the evolution of both structural and magnetic changes upon application of hydrostatic pressure the combination of LTE and magnetization measurements was used, since at high pressures, only very slight anomalies connected with structural transition were observed in the low-field magnetization measurements. In figure 9(a) we display the LTE of $Tb_5Si_2Ge_2$ (block symbols) at different values of the applied hydrostatic pressure. A large jump is observed in the LTE associated with the first-order M(FM) $\leftrightarrow$ O(I) (FM) crystallographic transition [50, 51] at $T_t \cong 93$ K (heating). This change in the structure takes place within the ferromagnetic phase since long-range ferromagnetism sets in at higher temperatures within the M structure [51]. The obtained T–P phase diagram is shown in figure 9(b), where the transition temperature values have been taken at the maximum derivative of the corresponding macroscopic property being monitored (only values upon heating the sample are displayed). Consistent with our systematic studies in the $Gd_5(Si_xGe_{1-x})_4$ series [47, 53], both T_t and T_C shift linearly with pressure to higher temperatures at rates $dT_t/dP = +2.64(6)$ K kbar^{-1} and, at $P < 8$ kbar, $dT_C/dP = +0.54(3)$ K kbar^{-1}; see figure 9(b). For the dT_C/dP determination, only values below 8 kbar have been used since both first-order (solid line) and second-order (dashed line) phase boundaries merge at a tricritical point at about 8.6 kbar. Above this pressure, a single and fully coupled magnetic–crystallographic transformation M(PM) $\leftrightarrow$ O(I) (FM) takes place.

Neutron powder diffraction experiments under a hydrostatic pressure of 9 kbar confirmed this behaviour. A zero-pressure thermal scan was also required in order to account for the effect of the pressure cell. In figure 10, strong differences in the three-dimensional thermodiffractogram in a selected angular range are clearly visible. The marked diffraction peaks are of pure magnetic origin coming from the M, O(I) or both [O(I) + M] crystallographic structures. The existence of M(FM) peaks are consistent with a previous study [10], and are

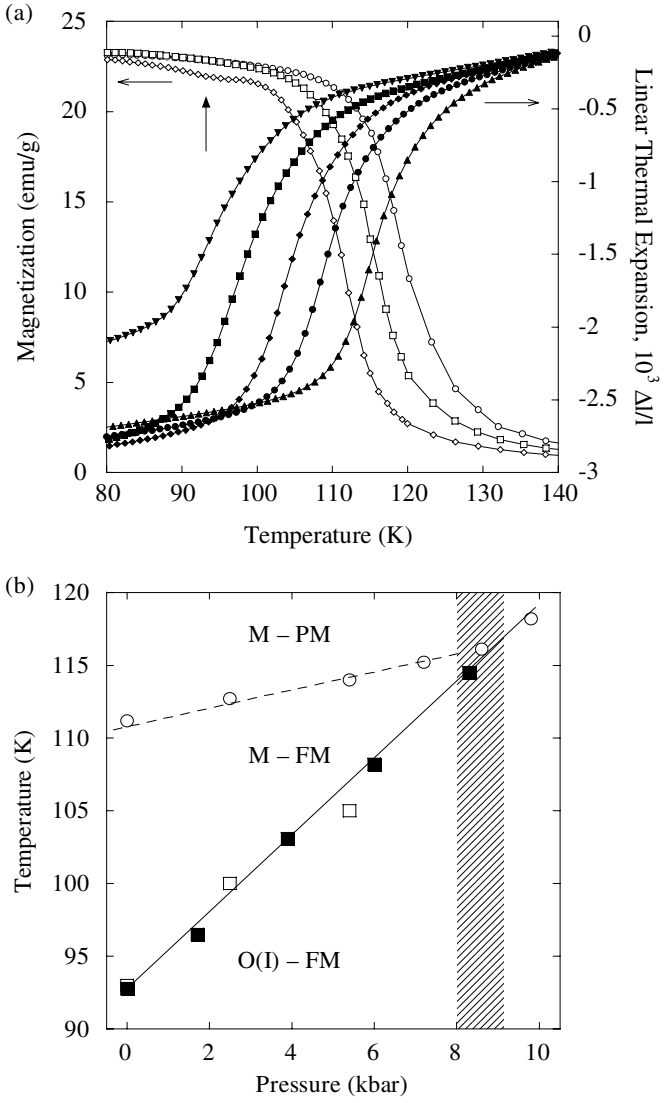

Figure 9. (a) Magnetization (open symbols) under 0 (◇), 7.2 (□), and 9.8 (○) kbar hydrostatic pressure, and linear thermal expansion (block symbols) under 0 (▼), 1.7 (■), 3.9 (◆), 6.0 (●), and 8.3 (▲) kbar of $Tb_5Si_2Ge_2$ measured on heating. The pressure values have been determined at the transition temperatures. (b) Temperature–pressure phase diagram as determined from magnetization (open circles and squares) and LTE (block squares) data. The dashed and solid lines depict the second-order and first-order transition lines, respectively [52].

essentially absent at 9 kbar (figure 10(b)). In figure 11, the integrated intensities of these three magnetic reflections as a function of temperature and under 9 kbar are shown. For the sake of comparison the results at 0 kbar have been included in the inset. These results demonstrate the existence of a fully coupled first-order M (PM) ↔ O(I) (FM) transformation below $\simeq$120 K as expected from the T–P phase diagram obtained from macroscopic measurements (figure 9(b)). It is also interesting to note that we have detected a small magnetic intensity of the M phase below $\simeq$114 K. This reflects the ferromagnetic ordering of the

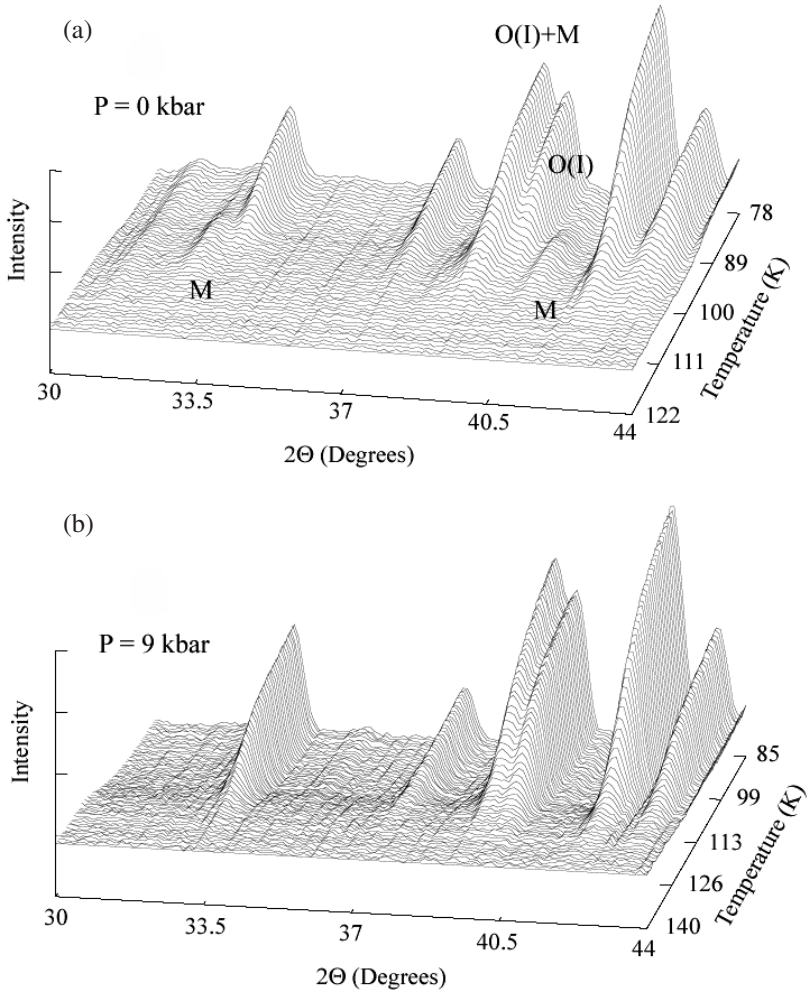

Figure 10. Thermodiffractogram of $Tb_5Si_2Ge_2$ in zero pressure (a) and under a 9 kbar hydrostatic pressure (b) in a selected angular range as measured in the high-intensity two-axis diffractometer D20 on cooling. The O(I), M, and O(I) + M diffraction peaks are purely magnetic in origin [52].

remaining fraction of M(PM) phase in the two-phase coexistence region O(I)(PM) + M(PM), in reasonable agreement with the shift of T_C with pressure as determined previously (note the one-order-of-magnitude difference in the integrated intensity of this peak since the fraction of M(PM) phase is rather small at this temperature, which makes it difficult to appreciate it in figure 11(b)). Therefore, the sequence of structural and magnetic transitions on cooling is as follows: M(PM) $\rightarrow$ M(FM) $\rightarrow$ [M(FM) + O(I)(FM)] $\rightarrow$ O(I)(FM) at $P = 0$ kbar, and M(PM) $\rightarrow$ [M(PM) + O(I)(FM)] $\rightarrow$ [M(FM) + O(I)(FM)] $\rightarrow$ O(I)(FM) at $P = 9$ kbar.

In conclusion, a coupling of the ferromagnetic transition with the structural change ($T_C = T_t$) was demonstrated and a tricritical point at approximately 8.6 kbar was determined in the temperature–composition phase diagram of $Tb_5Si_2Ge_2$. The tricritical point signals the collapse of the high-temperature second-order Curie transition [M(PM) $\leftrightarrow$ M(FM)] with the low-temperature first-order crystallographic transformation [M(FM) $\leftrightarrow$ O(I)(FM)]. The slopes of the corresponding phase boundaries have been determined as 0.54(3) and

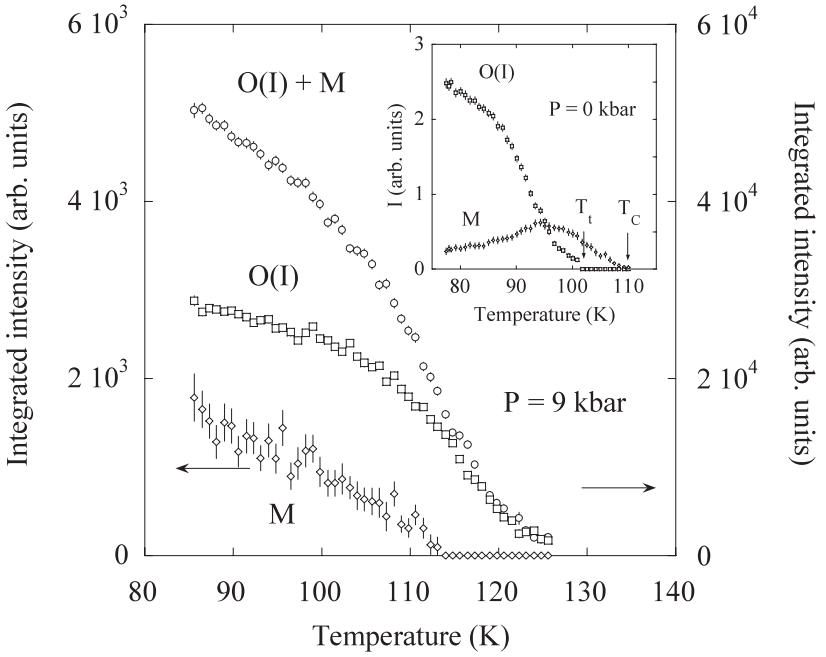

Figure 11. Temperature dependence of the integrated intensity of selected (marked in figure 10, the M peak used being the one at higher angles) O(I) (□), M (○), and O(I) + M (◇) purely magnetic diffraction peaks as determined from D20 data under a hydrostatic pressure of 9 kbar. This experiment was performed on cooling the sample. For comparison, the inset displays the thermal dependence of the O(I) and M magnetic peaks in zero pressure [52].

+2.64(6) K kbar^{-1}. This behaviour also has a remarkable impact on the magnetocaloric effect of this material that allowed quantifying the relative contributions of the change in the crystallographic and magnetic structures to the total entropy in a single alloy [52].

3.4. Non-collinear magnetic structure in Y_2Fe_{17} compound

Fe-rich intermetallic compounds, in particular the R_2Fe_{17} series of compounds (R = rare earth or Y), are well known for their peculiar magnetic behaviour. The crystal structure of R_2Fe_{17} is originated from the hexagonal RM_5 structure ($CaCu_5$ type) by substitution of one-third of the R atoms by pairs of Fe atoms (so called dumb-bells). Their uniaxial (hexagonal with heavy R or rhombohedral with light R) crystallographic structures can be considered as natural multilayer systems. The Fe atoms are located in four non-equivalent crystallographic positions within the unit cell. Although the R- and Fe-sublattices of the majority of compounds of the series order ferromagnetically (for light R and Y) and ferrimagnetically (for heavy R), non-collinear magnetic structures were observed in Ce_2Fe_{17}, Tm_2Fe_{17} and Lu_2Fe_{17} compounds in a limited temperature range [54, 55].

Non-collinear magnetism in iron has been a subject of intense research in the last few years. Both theoretical and experimental studies of this problem were intensified by the experimental works of Tsunoda [56, 57], who observed helical spin density waves in γ-Fe and γ-FeCo precipitates in Cu. Theoretical study of this problem has led to a great progress in a field of description of the spin dynamics in itinerant systems [58]. Recently, the existence of spin spiral ground state of γ-Fe was also studied theoretically [59, 60].

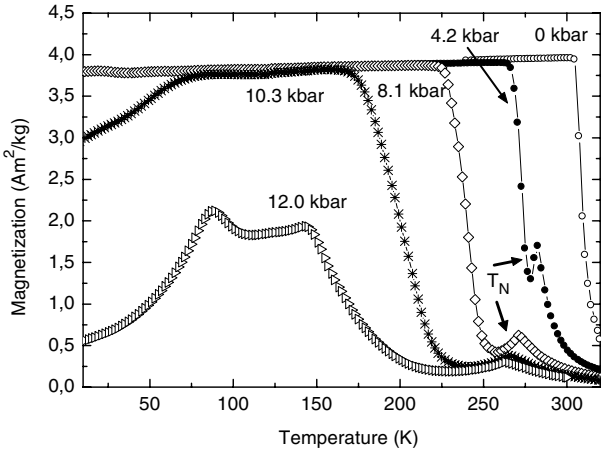

Figure 12. Temperature dependence of the magnetization of Y_2Fe_{17} at $\mu_0 H = 0.01$ T under pressure.

The magnetic and neutron measurements have confirmed that Y_2Fe_{17} has a collinear ferromagnetic structure ($T_C = 310$ K) with Fe magnetic moments ($\mu_{Fe} = 2.1\ \mu_B$) parallel to the basal ab plane. Since Y_2Fe_{17} has no 4f electrons, its magnetic properties served for a long time as a model for the magnetic behaviour of the Fe sublattice in the entire series of R_2Fe_{17} compounds. However, the destabilization of the collinear magnetism and the existence of a non-collinear ground state under applied pressure in Y_2Fe_{17} became a subject of controversy in the last decade [61].

Theoretical attempts to determine the relevant role of the interatomic Fe–Fe distances on hyperfine field, magnetization and critical temperature did not indicate the instability of the ferromagnetic phase [62]. On the other hand, indirect experimental indications about the existence of some form of pressure-induced non-collinear magnetic structure have been obtained by means of magnetization measurements at low fields, where a behaviour qualitatively similar to the one observed in the helimagmetic Ce_2Fe_{17} and Lu_2Fe_{17} compounds was obtained on Y_2Fe_{17} polycrystalline samples [61]. This effect, however, seemed to be largely influenced by the existence of structural disorder in the R_2Fe_{17} phases [63].

To confirm the existence of a non-collinear magnetic structure in Y_2Fe_{17} under high pressures, the temperature–pressure-field evolution of magnetic structures in Y_2Fe_{17} was studied using combined microscopic (neutron diffraction on both polycrystalline and single-crystalline samples) and macroscopic (magnetization, compressibility, thermal expansion) techniques under high hydrostatic pressure.

The temperature dependence of the low-field magnetization of Y_2Fe_{17} measured parallel to the easy a-axis at different pressures is presented in figure 12. At pressures above 4 kbar these curves exhibit two transitions similar to Ce_2Fe_{17} and Lu_2Fe_{17} [55, 64, 65]. A small maximum on the magnetization curve at high temperatures and pressures above 4 kbar characterizes the Neél temperature T_N. The sharp increase of the magnetization at these pressures with decreasing temperature indicates a transition to the ferromagnetic state.

The study of the magnetization parallel to the easy a-axis of Y_2Fe_{17} single crystals under pressure revealed a large initial decrease of the magnetization compared to that observed in other compounds of the series [66]. Moreover, the results of magnetization measurements under pressure of 9 kbar presented in figure 13 show that a metamagnetic transition to a ferromagnetic state occurs above $H_C = 0.44$ T (5 K) and 0.2 T (200 K). A field hysteresis as

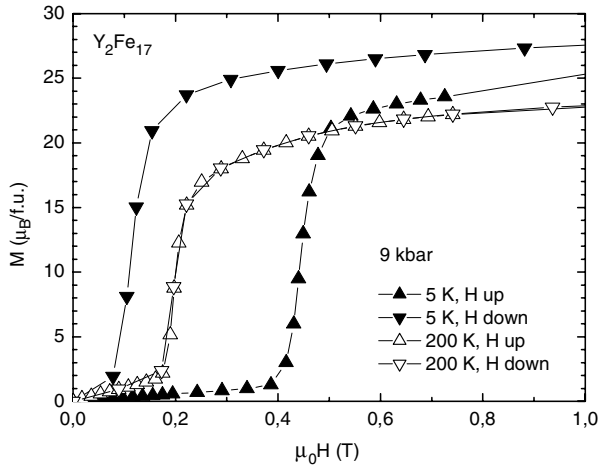

Figure 13. Magnetization isotherms at 5 and 200 K measured along the easy magnetization direction (a-axis) under pressure of 9 kbar.

large as 0.33 T is typical for magnetization isotherms at low temperatures whereas those at high temperatures do not present any remarkable hysteresis.

The neutron diffraction experiments performed on polycrystalline samples under pressures up to 20 kbar had severe experimental limitations because of the very high background level, caused by the incoherent scattering of the pressure cell whose volume is much higher than the sample; see figure 14(a). In spite of this experimental limitation a well visible 000^+ satellite was detected at 10 kbar in the limited temperature range 245–275 K. At pressures of 20 kbar the intensity of the 000^+ satellite significantly increases with the decreasing temperature down to 5 K. The presence of this satellite indicates the existence of incommensurate non-collinear magnetic structure in Y_2Fe_{17} under pressure. The temperature dependence of the propagation vector in Y_2Fe_{17} determined at 20 kbar together with the results of Lu_2Fe_{17} and Ce_2Fe_{17} measured at 5 kbar is presented in figure 14(b). The temperature behaviour of the propagation vector is similar for all three compounds: it changes non-monotonically with temperature and it exhibits a wide characteristic minimum around 125 K.

Anisotropy of both thermal expansion under pressure and compressibility along different crystallographic axes was observed in Y_2Fe_{17} [67]. The lattice becomes 'soft' along the c-direction. At 20 K the linear compressibility along c, $\kappa_c = 0.70 \pm 0.03$ Mbar^{-1}, is more than twice as large as that along a, $\kappa_a = 0.32 \pm 0.03$ Mbar^{-1}, and the volume compressibility $\kappa = 1.35 \pm 0.05$ Mbar^{-1} ($\kappa = 2\kappa_a + \kappa_c$). This anomalous decrease of the c parameter seems to be responsible for significant pressure-induced changes of the interlayer exchange interactions, which cause the change of magnetic structures, namely the pronounced increase of the propagation vector with pressure. This verifies an extremely high sensitivity of the interlayer exchange interactions to the pressure-induced changes of the lattice parameters.

Combined magnetic and neutron diffraction studies under high pressure proved that the ferromagnetic ground state of Y_2Fe_{17} is suppressed and the incommensurate antiferromagnetic phase is stabilized down to the lowest temperature under high pressures. This structure most probably has similar features to the structure observed in Lu_2Fe_{17}. The preliminary results of neutron diffraction under pressure performed on single-crystalline samples [68] confirmed the existence of the pressure-induced incommensurate helical structure with propagation vector along the c-axis. Magnetic moments in each layer of atoms (perpendicular to the c-axis)

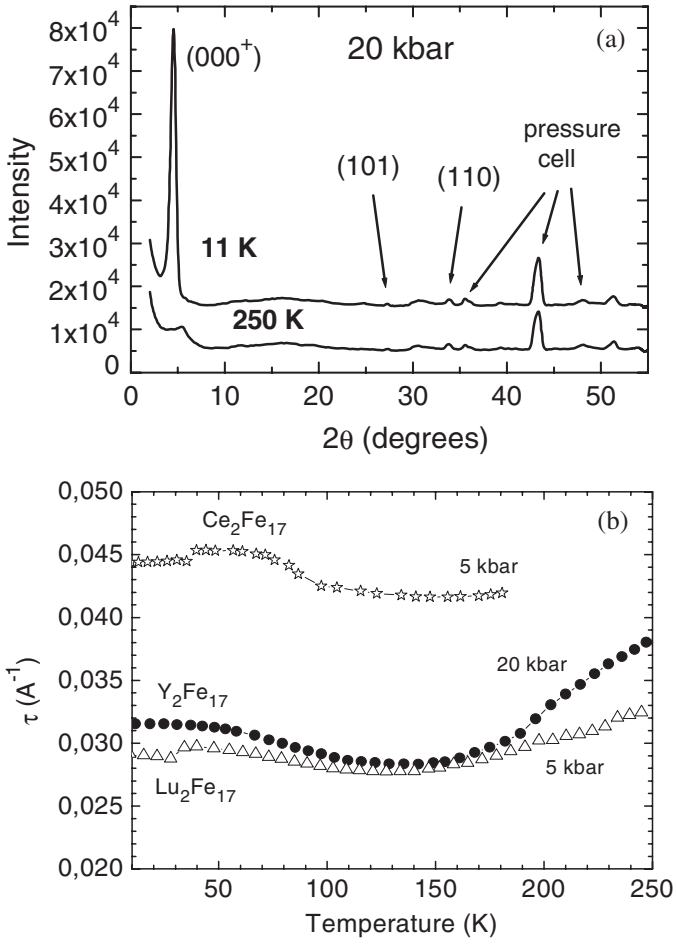

Figure 14. Diffraction patterns of Y_2Fe_{17} with observed 000^+ satellite and visible nuclear reflections at 20 kbar (a) and temperature dependence of the propagation vector of Lu_2Fe_{17} and Ce_2Fe_{17} measured at 5 kbar and of Y_2Fe_{17} measured at 20 kbar (b).

are parallel to each other but their direction changes from layer to layer. The pressure and temperature evolution of this non-collinear magnetic structure is rather complex and it can be attributed to intrinsic properties of the iron sublattice.

4. Summary

We have presented in this review several examples of the relevant role of neutron diffraction at medium pressure range to understand and characterize the nature of the relations between the changes of volume and the magnetic and magnetotransport properties.

A strong pressure effect exists on the electronic structure of mixed valence manganites with colossal magnetoresistance. The pressure-induced increase of T_C is the consequence of the enhancement of Zener interaction. The ferromagnetic phase is favoured with respect to the CO, resulting in a decrease of the resistivity under pressure. However, the effect is not large enough in the $^{18}O(La_{0.5}Nd_{0.5})_{2/3}Ca_{1/3}MnO_3$ sample to produce an In–Mt transition.

The combined studies of the magnetic phase diagram in $Tb_{1-X}Y_XMn_2$ compounds showed the pressure-induced suppression of first-order magnetic phase transition accompanied by the appearance of the local magnetic moment of Mn, coexistence of two different magnetic structure and the existence of the new, pressure-induced magnetic phase.

Complex studies of $RE_5Si_{4-X}Ge_X$ compounds showed different volume dependences of the temperatures of the first-order structural phase transitions and second-order magnetic transitions. As a consequence, pressure-induced coupling of the ferromagnetic transition with the structural change ($T_C = T_t$) was observed by neutron diffraction under pressure and a tricritical point in the vicinity of 8.6 kbar was determined in the temperature–pressure phase diagram of $Tb_5Si_2Ge_2$. This behaviour also has a remarkable impact on the magnetocaloric effect of this material that allowed quantifying the relative contributions of the change in the crystallographic and magnetic structures to the total entropy in a single alloy [52].

Magnetic, linear thermal expansion and neutron diffraction studies under high pressure proved that the ferromagnetic ground state of Y_2Fe_{17} is suppressed and the incommensurate antiferromagnetic phase is stabilized down to the lowest temperature under high pressures. The preliminary results of neutron diffraction under pressure performed on single-crystalline samples [68] confirmed that negative interlayer interactions are enhanced under pressure. The complex pressure–temperature–field behaviour of the pressure-induced helical magnetic phase has to be attributed to intrinsic properties of the iron sublattice.

Acknowledgment

We acknowledge the support of AS CR within the Project No AV0 Z10100521.

References

[1] Kamarád J 2001 *Encyclopedia of Materials: Science and Technology* (Oxford: Elsevier Science) p 4976
[2] Schilling J S 1984 *High Pressure in Science and Technology* vol 22, ed C Homan, R K MacCrone and E Whalley (Amsterdam: Elsevier Science) p 7 (Part I)
[3] Ibarra M R and De Teresa J M 1998 *Colossal Magnetoresistance, Charge Ordering and Related Properties of Manganese Oxides* ed C N R Rao and B Raveau (Singapore: World Scientific) p 83
[4] Arnold Z, Kamenev K, Ibarra M R, Algarabel P A, Marquina C, Blasco J and Garcia J 1995 *Appl. Phys. Lett.* **67** 2875
[5] Neumeier J J, Hundley M F, Thompson J D and Heffner R H 1995 *Phys. Rev.* B **52** R7006
[6] Fontcuberta J, Martinez B, Seffar A, Pinol S, GarciaMunoz J L and Obradors X 1996 *Phys. Rev. Lett.* **76** 1122
[7] Shiga M, Wada H and Nakamura Y 1983 *J. Magn. Magn. Mater.* **31–34** 119
[8] Spichkin Y I, Pecharsky V K and Gschneidner K A 2001 *J. Appl. Phys.* **89** 1738
[9] Brouha M, Buschow K H J and Miedema A R 1973 *IEEE Trans. Magn.* **10** 182
[10] Kamarád J, Kamenev K V and Arnold Z 1996 *High Pressure in Science and Technology* (Singapore: World Scientific) p 51
[11] Kamarád J, Machátová Z and Arnold Z 2004 *Rev. Sci. Instrum.* **75** 5022
[12] Rodriguez-Carvajal J 1993 *Physica* B **192** 55
[13] Zener C 1955 *Phys. Rev.* **82** 1403
[14] Anderson P W and Hasegawa H 1955 *Phys. Rev.* **100** 675
[15] Millis A J, Littlewood P B and Shraiman B I 1995 *Phys. Rev. Lett.* **74** 5144
[16] Hwang H Y, Cheong S W, Radaelli P G, Marezio M and Batlogg B 1995 *Phys. Rev. Lett.* **75** 914
[17] Urushibara A, Moritomo Y, Arima T, Asamitsu A, Kido G and Tokura Y 1995 *Phys. Rev.* B **5** 14103
[18] Zhao G-M, Conder K, Keller H and Miiller K A 1996 *Nature* **381** 676
[19] Ibarra M R *et al* 1995 *Phys. Rev. Lett.* **75** 3541
[20] Radaelli P G *et al* 1995 *Phys. Rev. Lett.* **75** 4488
[21] De Teresa J M *et al* 1995 *Phys. Rev.* B **54** 1187
[22] Kusters R M, Singleton J, Keen D A, McGreevy R and Hayes W 1989 *Physica* B **155** 362
[23] De Teresa J M *et al* 1996 *Phys. Rev. Lett.* **7** 3392

[24] Zhao G-M *et al* 1996 *Nature* **38** 676
[25] Jin S, O'Bryan H M, Tiefel T H, McCormack M and Rhodes W W 1995 *Appl. Phys. Lett.* **6** 382
[26] Tomioka Y *et al* 1995 *Phys. Rev. Lett.* **74** 5108
[27] Rao G H *et al* 1997 *Phys. Rev.* B **55** 3742
[28] Zhou J S *et al* 1996 *Nature* **381** 770
[29] Zhao G-M *et al* 1997 *Solid State Commun.* **104** 57
[30] De Teresa J M *et al* 1997 *Nature* **386** 256
[31] De Teresa J M *et al* 1996 *Phys. Rev.* B **54** R12689
[32] Ibarra M R *et al* 1998 *Phys. Rev.* B **57** 7446
[33] Ibarra M R and Algarabel P A 1994 *Phys. Rev.* B **50** 4196
[34] Adroja D T, Rainford B D, De Teresa J M, del Moral A, Ibarra M R and Knight K S 1995 *Phys. Rev.* B **52** 12790
[35] Ibarra M R, Marquina C, Algarabel P A, De Teresa J M, Ritter C and del Moral A 1994 *Proc. 13th Int. Workshop on Rare Earth Magnets and their Applications (Birmingham 1994)* ed C A F Manwaring *et al* p 127
[36] Shiga M 1988 *Physica* B **149** 293
[37] Mondal S, Cywinski R, Kilcoyne S H, Rainford B D and Ritter C 1992 *Physica* B **180/181** 108
[38] De Teresa J M, Ibarra M R, Ritter C, Marquina C, Arnold Z and del Moral A 1995 *J. Phys.: Condens. Matter* **7** 5643
[39] Corliss L M and Hastings J M 1964 *J. Appl. Phys.* **35** 1051
[40] Brown P J, Ouladdiaf B, Ballou R, Deportes J and Markosyan A S 1992 *J. Phys.: Condens. Matter* **4** 1103
[41] De Teresa J M, Ritter C, Ibarra M R, Arnold Z, Marquina C and del Moral A 1996 *J. Phys.: Condens. Matter* **8** 8385
[42] Pecharsky V K and Gschneidner K A Jr 1997 *Phys. Rev. Lett.* **78** 4494
Pecharsky V K and Gschneidner K A Jr 1997 *Appl. Phys. Lett.* **70** 3299
Pecharsky V K and Gschneidner K A Jr 1997 *J. Magn. Magn. Mater.* **167** L179
[43] Pecharsky V K and Gschneidner K A Jr 2001 *Adv. Mater.* **13** 683
[44] Morellon L *et al* 1998 *Phys. Rev.* B **58** R14721
Morellon L *et al* 2000 *Phys. Rev.* B **62** 1022
[45] Morellon L *et al* 1998 *Appl. Phys. Lett.* **73** 3462
Morellon L *et al* 2001 *J. Magn. Magn. Mater.* **237** 119
Levin E M, Pecharsky V K and Gschneidner K A Jr 1999 *Phys. Rev.* B **60** 7993
[46] Choe W *et al* 2000 *Phys. Rev. Lett.* **84** 4617
[47] Magen C *et al* 2003 *Phys. Rev. Lett.* **91** 207202
[48] Magen C *et al* 2003 *J. Phys.: Condens. Matter* **15** 2389
[49] Morellon L *et al* 2001 *Appl. Phys. Lett.* **79** 1318
[50] Ritter C *et al* 2002 *Phys. Rev.* B **65** 094405
[51] Morellon L *et al* 2003 *Phys. Rev.* B **68** 024417
[52] Morellon L 2004 *Phys. Rev. Lett.* **93** 137201
[53] Morellon L *et al* 2004 *J. Phys.: Condens. Matter* **16** 1623
[54] Givord D and Lemaire R 1974 *IEEE Trans. Magn.* **10** 109
[55] Prokhnenko O, Ritter C, Arnold Z, Isnard O, Kamarád J, Pirogov A, Teplykh A and Kuchin A 2002 *J. Appl. Phys.* **92** 385
[56] Tsunoda Y 1989 *J. Phys.: Condens. Matter* **1** 10427
[57] Tsunoda Y, Nishioka Y and Nicklow R M 1993 *J. Magn. Magn. Mater.* **128** 133
[58] Sandratskii L M 1998 *Adv. Phys.* **47** 91
[59] Knöpfle K, Sandratskii L M and Kübler J 2000 *Phys. Rev.* B **62** 5564
[60] Sjöstedt E and Nordström L 2002 *Phys. Rev.* B **66** 014447
[61] Nikitin S A, Tishin A M, Kuźmin M D and Spichkin Yu I 1991 *Phys. Lett.* A **153** 155
[62] Beurle T and Fähnle M 1992 *J. Magn. Magn. Mater.* **110** L29
[63] Arnold Z, Kamarád J, Algarabel P A, Garcia-Landa B and Ibarra M R 1994 *IEEE Trans. Magn.* **30** 619
[64] Buschow K H J and van Wieringen J S 1970 *Phys. Status Solidi* **42** 231
[65] Givord D and Lemaire R 1972 *C. R. Acad. Sci. Paris* **274** 1166
[66] Kamarád J, Mikulina O, Arnold Z, García-Landa B and Ibarra M R 1999 *J. Appl. Phys.* **85** 4874
[67] Arnold Z, Kamarád J, Prokhnenko O, Ritter C, Eto T, Honda F, Oomi G and García-Landa B 2002 *High Pressure Res.* **22** 175
[68] Prokhnenko O *et al* 2005 *Phys. Rev. Lett.* **94** 107201